Nanoscale Advances

Accepted Manuscript

This article can be cited before page numbers have been issued, to do this please use: S. Jahani, J. Morin and A. M. Ritcey, *Nanoscale Adv.*, 2026, DOI: 10.1039/D6NA00126B.

ROYAL SOCIETY OF CHEMISTRY

rsc.li/nanoscale-advances

View Article Online
DOI: 10.1039/D6NA00126B

Facile fabrication of hollow carbon nanomaterials by directed polymerization of butadiyne on the surface of reverse micelles

Sara Jahani, Jean-François Morin, Anna M. Ritcey**

Département de chimie and Centre de Recherche sur les Matériaux Avancés (CERMA)

1045 Ave de la Médecine, Université Laval, Québec, Canada G1V 0A6

E-mails: Jean-Francois.Morin@chm.ulaval.ca; Anna.Ritcey@chm.ulaval.ca

View Article Online
DOI: 10.1039/D6NA00126B

ABSTRACT

Uniform hollow carbon nanoparticles (CNPs) of different shapes were prepared by a reverse microemulsion polymerization method. The main advantage of this method is the ability to control the precise shape of the nanoparticles. The CNPs were prepared by the room temperature polymerization of a butadiyne monomer on self-assembled surfactant templates formed in the ternary system containing sodium bis (2-ethylhexyl)sulfosuccinate (AOT), water, and hexane. The size and shape (spherical, cylindrical and lamellar phase) of the aggregated surfactant template depend on the composition of the ternary system, which varies primarily through the water content parameter. After template removal by simple washing, the CNPs were studied by morphological analysis (transmission electron microscopy) and chemical characterization with a variety of methods, including energy dispersive X-ray spectroscopy, X-ray photoelectron spectroscopy, Auger electron spectroscopy and Raman spectroscopy. Depending on the template shape, CNPs were obtained in the form of hollow spheres, hollow rods or lamellar sheets. Results from various characterization techniques indicate that the obtained nanomaterials are primarily composed of sp^2 hybridized carbon.

KEYWORDS: Carbon nanomaterials, Template polymerization, Self-assembly, Polyynes, Solution-phase synthesis, Soft-templating, Morphology control, Nanorods, Nanospheres

1. INTRODUCTION

View Article Online
DOI: 10.1039/D6NA00126B

Carbon nanomaterials are of interest for multiple applications including bioimaging, drug delivery, sensing, and photocatalysis. Certain carbon nanomaterials, such as zero dimensional fullerenes, one-dimensional carbon nanotubes and two-dimensional graphene, are composed entirely of sp^2 carbon atoms, and have attracted much attention because of their unique physical and structural properties.[1] Carbon nanoparticles (CNPs) are a well-studied member of the wider class of carbon nanomaterials because they are inexpensive, non-toxic, and safe.[2] Other advantages of CNPs, such as high biocompatibility, easy surface functionalization, and environmental friendliness, have led to their use in very important fields such as drug delivery in the human body and as catalysts in green chemistry.[3] The main obstacle to the further development of CNPs is the difficulty of controlling their size and shape, as well as the exact nature of carbon-carbon bonding within them. The majority of synthetic methods developed to date involve the pyrolysis of various abundant and inexpensive sources of carbon, such as sugars,[4] plants,[5] fruit juice,[6] and coffee.[7] After pyrolysis, the CNPs are extracted from the resulting soot, a process that is often tedious and inefficient, and produces very small quantities of polydisperse nanoparticles with poorly defined properties. In addition, this high-temperature method does not allow for the control over the size and the shape of the nanoparticles.[8] In an effort to overcome this lack of control, Gu and coworkers reported the use of Metal-Organic-Frameworks (MOFs) in a hard template-assisted method to synthesize CNPs.[9] They loaded glucose as a carbon source into the MOF before heating at 200 ˚C for two hours to produce the CNPs. After the formation of the CNPs, the hard template is removed by etching, adding an additional step to the process. Furthermore, the MOF hard template is restricted to very small sizes and does not allow for the preparation of particles of different shapes

View Article Online
DOI: 10.1039/D6NA00126B

or hollow structures.[10] Another challenge of the hard template approach is that the scale up for industrial applications is very difficult.

Since high temperature synthetic methods generally lead to the formation of amorphous, disordered CNPs, without a well-defined shape, and which often tend to aggregate during their preparation and isolation,[11] the current study introduces a soft template method that can be employed at ambient conditions. The soft template method, which is also called the self-assembly method,[12] has attracted much attention for nanoparticle synthesis but has not yet been used for the preparation of CNPs. This approach is inexpensive and relatively simple, and, importantly, provides access to nanoparticles of different sizes and shapes[12]. The soft template method employs amphiphile molecules as the structure-directing agent. Examples include deoxyribonucleic acid (DNA),[13] surfactants,[14] and liquid crystals.[15] Under appropriate conditions, amphiphilic molecules self-assemble into structures such as emulsions, lamella, vesicles or micelles which are used as templates that organize and control the growth of guest structures. To date, this method has been used for the production of a large variety of nanomaterials including polypyrrole nanotubes,[16] poly(3,4-ethylene dioxythiophene) (PEDOT) nanotubes,[17] $BaSO_4$ nanofilaments,[18] $BaWO_4$ nanorods,[19] polyaniline nanofibers,[20] silica nanospheres[21] and gold nanoparticles.[22]

In the present report, different self-assembled structures are created by varying the composition of a ternary surfactant/water/solvent system and used as soft templates for the polymerization of butadiyne to produce carbon nanomaterials. This work builds on our recently reported synthesis of twisted graphene within a lamellar surfactant template.[23] Here we extend this synthetic approach to prepare CNPs of varying shape by modifying the self-assembled phase of the surfactant template

View Article Online
DOI: 10.1039/D6NA00126B

on which the carbon particles grow. These findings support the hypothesis that the carbon nanomaterials form through the spontaneous decomposition of unstable polyynes, which are direct products of the polymerization process.[24–26]

2. EXPERIMENTAL SECTION

2.1. Materials

Sodium bis(2-ethylhexyl) sulfosuccinate (AOT), copper (II) triflate ($Cu(OTf)_2$) were purchased from Sigma Aldrich. The solvents including hexane and methanol (99.9%) are obtained from Fisher Scientific. The 1,4-bis(trimethylsilyl)butadiyne monomer was synthesized following the method of Jones *et al.*[27] Details are provided in the Supporting Information section.

2.2. Preparation of surfactant self-assembled structures

The self-assembled templates were prepared by dispersing an aqueous solution of $Cu(OTf)_2$ in a solution of AOT dissolved in hexane with simple mechanical stirring for 10 minutes. The Cu^{+2} concentration in the aqueous solution was kept constant at 7×10^{-3} M for all experiments. Different template structures were obtained by varying the molar ratios of the three components (surfactant, solvent, aqueous solution) of the ternary system. The composition and water content (W), defined as the molar water to surfactant ratio, of the various samples investigated are provided in Table 1.

Table 1. Chemical composition and water content of templates mixtures

View Article Online
DOI: 10.1039/D6NA00126B

Sample	Component quantity (mmole)			Water content (W)
	AOT	Hexanes	Water*	
a	1.1	76	2.2	2
b	2.5	42.9	25	10
c	3.7	58	48	13
d	4.5	174.1	108	24

* added as a solution containing 7×10^{-3} M Cu^{+2}

2.2.1 Determination of volume fractions

In order to compare the investigated mixtures with literature phase diagrams, molar compositions were converted to volume fractions following the method reported by Lisiecki *et al.*[28,29] First, the volume occupied by the surfactant (V_{AOT}) is given by

$$V_{AOT} = n_{AOT}.N_{Av}.v_{AOT}.10^{-24}cm^3 \quad [1]$$

where the $n_{AOT,}$ N_{Av} and v_{AOT} are the number of moles of surfactant, Avogadro's number and the volume of an AOT molecule, respectively. The volume of an AOT molecule was assumed to be constant and equal to 639Å^3.[28]

Similarly, the water volume (V_W) is calculated as

$$V_W = n_W.N_{Av}.v_W.10^{-24}cm^3 \quad [2]$$

where $n_{w,}$ and v_w are the number moles of water and the volume of a single water molecule, respectively. The volume occupied by a water molecule in a reverse micelle is assumed to follow

View Article Online
DOI: 10.1039/D6NA00126B

the logarithmic law provided in equation [3] and ranges from 15 to 30 Å^3 for water contents (W) in the range of 1-20.[28]

$$V_W = \frac{ln\, W}{ln\, 1.1273} + 15 \qquad [3]$$

The total volume of the template, obtained from the sum of V_{AOT}, V_W and the volume of hexanes employed to prepare the mixture, allows for the calculation of the volume fractions (φ) of each of three template components, which are provided in Table 2.

Table 2. Template component volume fractions (φ) for the various samples

Sample	Volume fraction (φ)		
	AOT	Hexane	Water
A	0.05	0.94	0.01
B	0.10	0.84	0.06
C	0.14	0.75	0.11
D	0.15	0.63	0.22

2.3. Polymerization step: Synthesis of carbon nanomaterials

Carbon nanomaterials were obtained in one step by the polymerization of butadiyne (Figure 1) followed by the spontaneous decomposition of the reaction product. 1,4-Bis(trimethylsilyl)

View Article Online
DOI: 10.1039/D6NA00126B

butadiyne (50 mg, 2.6 x 10^{-4} mol) and potassium fluoride (KF, 30 mg, 5.0 x 10^{-4} mol) were added to the various template solutions described in Table 1. The fluoride salt is included to remove the protecting trimethylsilyl groups from butadiyne prior to polymerization. The resulting mixture was added to a small flask and stirred for 3 hours at room temperature and atmospheric pressure. Under these conditions, the reaction medium rapidly turned black, indicating the formation of solid carbon materials that are isolated by centrifugation. Residual AOT was removed and the CNPs were purified by centrifugation at 5000 rpm for 20 minutes, at room temperature, followed by redispersion in methanol. Five centrifugation/dispersion cycles were performed.

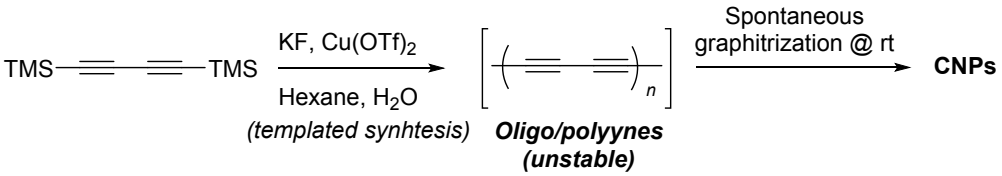

Figure 1. Synthetic schema for the preparation of carbon nanomaterials from 1,4-bis(trimethylsilylacetylene).

2.4. Characterization

Samples for energy-dispersive X-ray spectroscopy (EDS), X-ray photoelectron spectroscopy (XPS), X-ray induced Auger electron spectroscopy (XAES) and Raman spectroscopy analyses were prepared by depositing a few drops of a suspension of CNPs in methanol on small pieces of a silicon wafer. The surface composition was assessed by X-ray photoelectron spectrometer (XPS) using a Physical Electronics PHI 5600-ci equipment (Eden Prairie, MN, USA). XPS and XAES

View Article Online
DOI: 10.1039/D6NA00126B

spectra were acquired using an achromatic aluminum X-ray source (Al Kα = 1486.6 eV) without charge compensation. The scan area was 0.5 mm² with a collection angle of 45˚ relative to the surface normal. The curve fitting procedure of the components underlying the C1s peaks was performed by means of a least-square minimization procedure employing Gaussian–Lorentzian functions and a Shirley-type background, and the reference was set to the carbon (C1s) peak at 285.0 eV.

The EDS analysis was performed with a FEI Inspect F50 scanning electron microscope. For the EDS analysis, Au and Pd were used to coating the particles for better conductivity. All samples were dried under vacuum before analysis.

Raman spectra of CNPs were acquired using a Bruker Senterra II Raman microscope with a 633 nm laser and 50× objective.

Samples for transmission electron microscopy (TEM) and electron diffraction measurements were prepared by depositing a drop of a CNP suspension in methanol on carbon-coated nickel TEM grids and examined with a JEOL1230 microscope operated at 80 kV.

Template micellar solutions were characterized by dynamic light scattering (DLS). DLS was performed using a Malvern (Zetasizer Nano ZS) instrument equipped with a 633 nm laser and photodiode detector.

Attenuated total reflection (ATR) infrared spectroscopy was used to investigate the sample of carbon nanoparticles directly without special preparation. The ATR spectra were recorded on a Nicolet spectrometer and a golden gate diamond accessory. All spectra were recorded at 25 ˚C with 64 scans at 4 cm^{-1} resolution.

View Article Online
DOI: 10.1039/D6NA00126B

3. RESULTS AND DISCUSSION

3.1 Morphology of the prepared carbon nanomaterials

TEM images of synthesized carbon nanomaterials for samples **a**, **b**, **c**, and **d** are presented in Figure 2. The images clearly show that carbon nanomaterials of different morphologies, including nanospheres, nanoellipsoids, nanorods and honeycomb-like layers, are obtained. Since the various samples differ only in the proportions of water, surfactant and solvent employed, which are known to strongly influence the shape of the self-assembled surfactant structures, the results suggest that these structures do indeed serve as a template for the polymerization reaction.

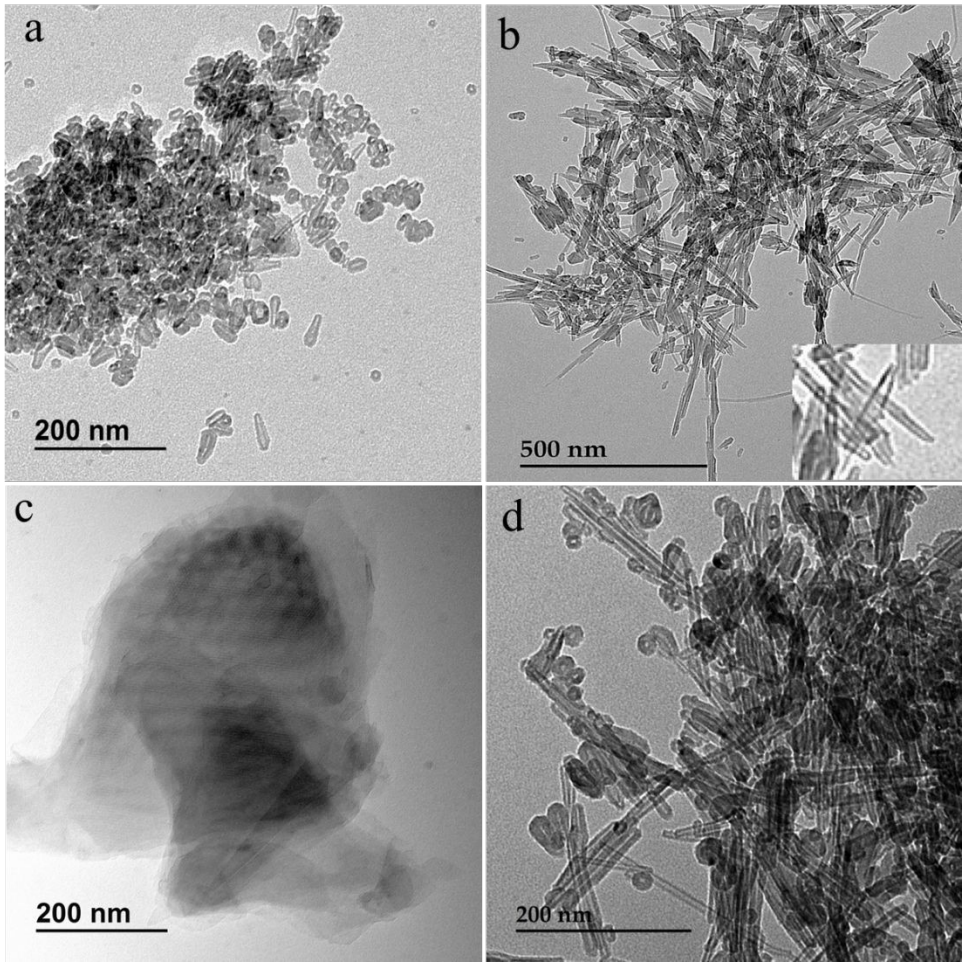

View Article Online
DOI: 10.1039/D6NA00126B

Figure 2. TEM images of carbon nanomaterials with distinct morphologies prepared at different water content (W): (a) hollow carbon nanospheres (W=2), (b) hollow carbon nanorods with a magnified inset (W=10), (C) carbon honeycomb-like layers (W=13), and (d) a mixture of hollow carbon nanorods and nanospheres (W=24). The materials were prepared from the template compositions provided in Table 1.

3.2 Phase behavior of the AOT/water-Cu^{2+}/hexane system

The ternary phase diagram for the specific AOT/water-Cu^{2+}/hexane system employed in this study has not yet been reported in the literature. It is important to note that copper (II) has been included in the reaction medium because it is required to catalyze the polymerization reaction. The addition of salt, and divalent cations in particular, significantly modifies the phase behavior of anionic surfactants through a reduction in the electrostatic repulsion between headgroups that, in turn, modifies the surfactant critical packing parameter [30]. The template compositions selected for this study were based on the phase diagram reported by Lisiecki *et al.*[29] for $Cu(AOT)_2$/water/isooctane mixtures, which correspond to the closest analogous system available in the literature. The compositions of the templates employed for the preparation of samples **a-d** are represented on the ternary composition diagram shown in Figure 3. By analogy to the phase diagram established for the $Cu(AOT)_2$/water/isooctane system [28,29], these four compositions correspond to the formation of spherical inverse micelles, cylindrical inverse micelles, lamellar phases, and a mixture of spherical and cylindrical inverse micelles, respectively.

View Article Online
DOI: 10.1039/D6NA00126B

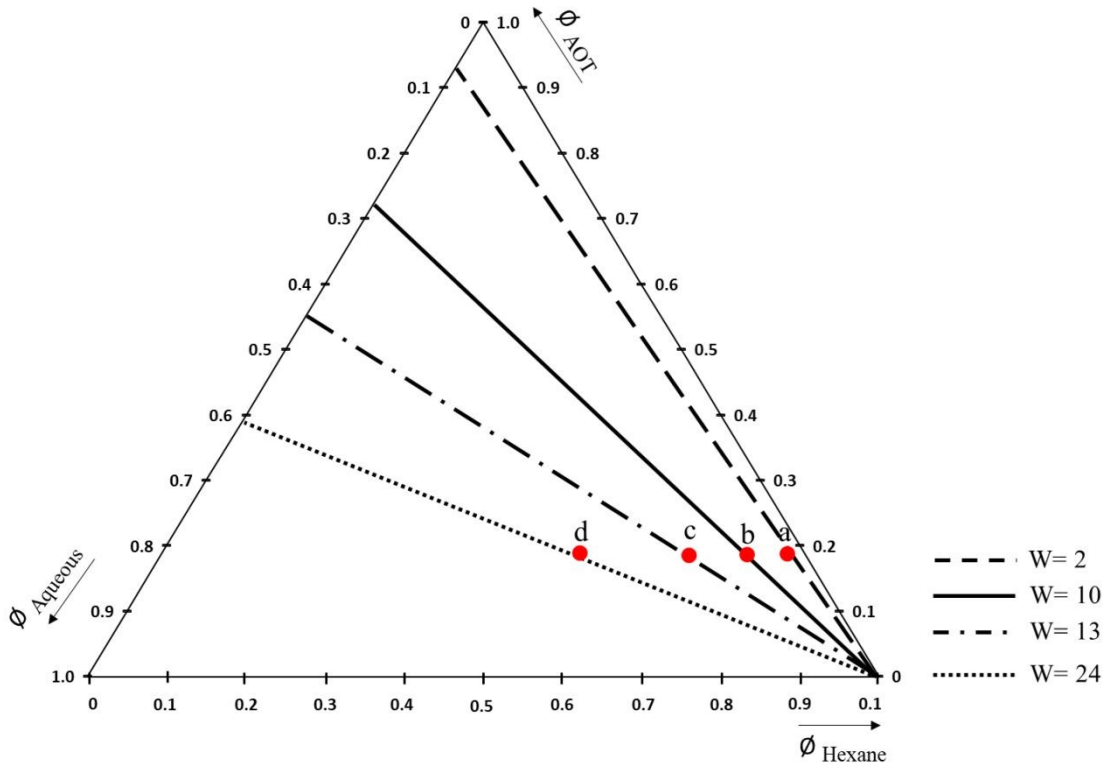

Figure 3. Ternary composition diagram for AOT /aqueous copper (II) triflate / hexane mixtures. Compositions are expressed in terms of volume fractions and points labeled **a**, **b**, **c** and **d** correspond to the compositions employed as templates for the synthesis of CNPs. Lines correspond to compositions of constant water/surfactant molar ratios, W, as indicated.

3.3 Critical packing parameter and aggregate shape

The critical packing parameter of a surfactant molecule corresponds to the ratio of the cross sectional area of the hydrophobic tail to the area of the polar head group[31]. This parameter therefore defines the curvature of the water/oil interface in a microemulsion and the shape of the surfactant self-assembled structures. The relationship between the critical packing parameter and the shape of surfactant assemblies is summarized in Table S1 of the supporting information.

View Article Online
DOI: 10.1039/D6NA00126B

For a given surfactant, the water to surfactant molar ratio, W, (also referred to as the water content) is the most important parameter that affects the shape of self-assembled structures in microemulsion systems[32]. Lines corresponding to various water contents, ranging from 2 to 24, are plotted in Figure 2. At low water content, AOT forms inverse micelles because the volume occupied by the two hydrophobic chains is large relative to the size of the polar head group. As water content is increased, the area occupied by the polar headgroups becomes larger due to an increase in hydration [28]. The resulting change in the critical packing parameter leads to the transformation of spherical micelles to cylindrical micelles and cylindrical micelles to a lamellar structure at progressively higher water contents[29]. The transformations are shown schematically in Figure 4.

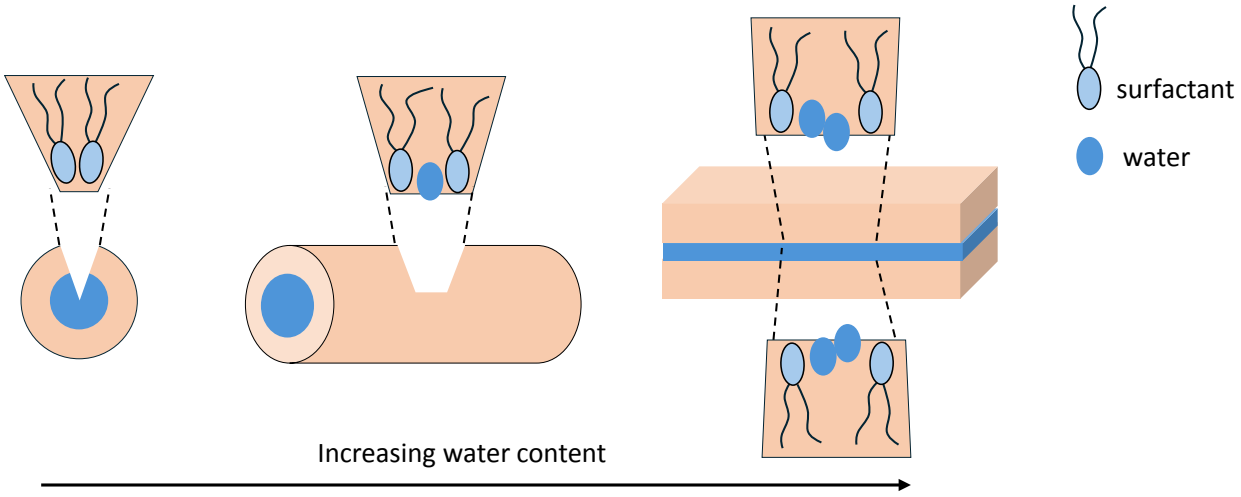

Figure 4: Schematic representation of the change in surfactant aggregate shape with increasing water content.

As noted above, at the highest water content investigated (W = 24, sample **d**), a mixture of spheres and cylinders are obtained. Although the transition from lamellae to spheres and cylinders

View Article Online
DOI: 10.1039/D6NA00126B

with increasing water content cannot be rationalized with the simple head group hydration argument presented above, it is consistent with SAXS measurements reported for the analogous $Cu(AOT)_2$/water/isooctane system [29].

3.4 Evidence for soft-templating

A summary of the relationship between the predicted surfactant structure and the shape of synthesized carbon nanomaterials is provided in Table 3. Even though the phase diagram for the specific system investigated here has yet to be established, the correspondence between the predicted template structure and the carbon nanostructures obtained by butadiyne polymerization is striking and supports the hypothesis that the surfactant self-assembled structures serve as templates during the polymerization reaction.

Table 3: Correlation of predicted template structures and morphology of synthesized carbon nanomaterials at various water contents

Sample	Water content (W)	*Predicted template structure	TEM images of the obtained carbon nanomaterials
a	2	Spherical micelles 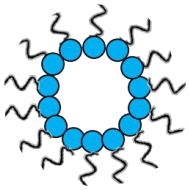	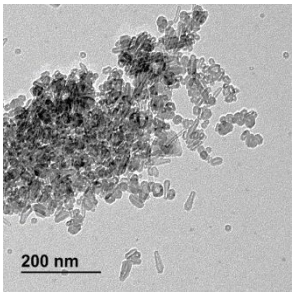

View Article Online
DOI: 10.1039/D6NA00126B

b	10	Cylindrical micelles 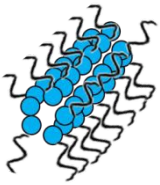	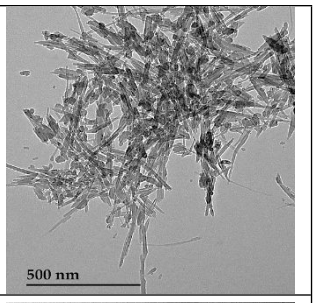
c	13	Lamellar phase 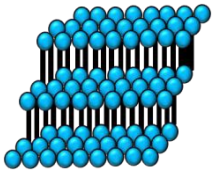	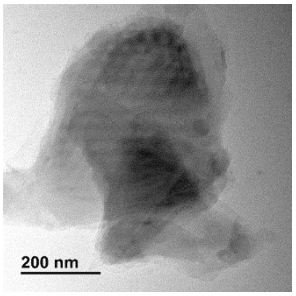
d	24	Mixture of spherical and cylindrical micelles 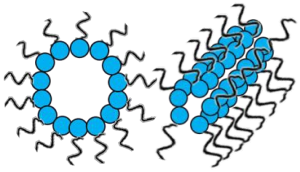	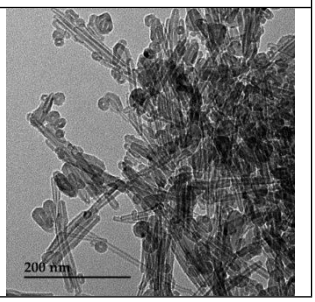

* Based on the phase diagram reported in refs 27 and 29

A second observation that strongly supports the hypothesis of templated polymerization is the fact that the resulting carbon nanostructures are hollow. Given that the monomer is soluble in the organic phase whereas the copper ions required to catalyze the polymerization reaction are present in the aqueous phase, it can be predicted that the polymerization reaction will take place around the micelles at the water-organic interface. A schematic representation of the templated production of different shapes of carbon nanomaterials is shown in Figure 5.

View Article Online
DOI: 10.1039/D6NA00126B

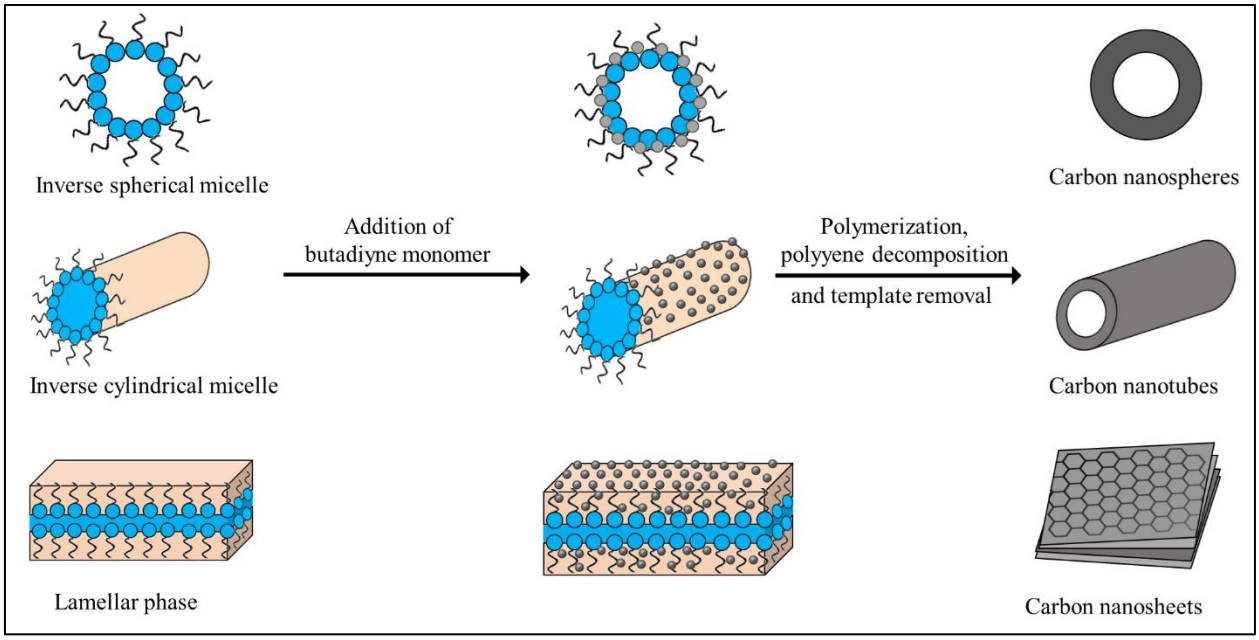

Figure 5. Scheme representation of the synthesis of carbon nanostructures in a self-assembled surfactant template.

3.5 Dimensions of the carbon nanoparticles

The dimensions of the synthesized carbon nanoparticles, as estimated from TEM images, are summarized in Table 4. Measurements were performed on a minimum of 30 particles and size distribution histograms are provided in Figures S1-S3.

Table 4: Dimensions of the synthesized hollow carbon nanoparticles

	Morphology	Inner diameter*	Outer diameter*	Rod length
a	Hollow spheres and ellipsoids	4.5-6 nm	5-6 nm	-
b	Hollow rods	2-3 nm	1.5-2 nm	50-100 nm

View Article Online
DOI: 10.1039/D6NA00126B

d	Hollow spheres and rods	2-3 nm for rods 3-4 nm for sphere	4-5 nm for rods 7-9 nm for spheres	130-160 nm

* Dimensions along the short axis in the case of ellipsoids and rods.

The hydrodynamic diameter of the spherical micelles employed as the template for sample **a** was evaluated by dynamic light scattering (DLS) to be approximately 4.5 nm (Figure S4). This micelle size corresponds very well with the inner dimensions of the hollow carbon nanospheres and further supports the hypothesis that the carbon nanomaterials are formed by polymerization around the template structures. However, since it is known that an increase in water content also leads to the formation of elliptical and cylindrical micelles, the hydrodynamic diameters determined by DLS must be interpreted with care. In fact, the CNPs of sample **a** do not all have a spherical shape, implying that elongated micelles are either already present in the template at W = 2 or form during the polymerization process.

3.6 Characterization of carbon nanomaterials

3.6.1 Electron diffraction

The electron diffraction patterns for samples **a** and **c** are provided in Figure 6. The diffraction pattern of sample **a** shows diffuse rings indicative of an amorphous structure. Samples **b** and **d** exhibit similar patterns (not shown), indicating that they are also composed of amorphous materials. In contrast, the diffraction pattern of sample **c** shows well-defined diffraction spots characteristic of a highly ordered structure. As discussed in detail in another report[23], this

View Article Online
DOI: 10.1039/D6NA00126B

diffraction pattern indicates that sample **c** is composed of twisted stacks of crystalline graphene layers.

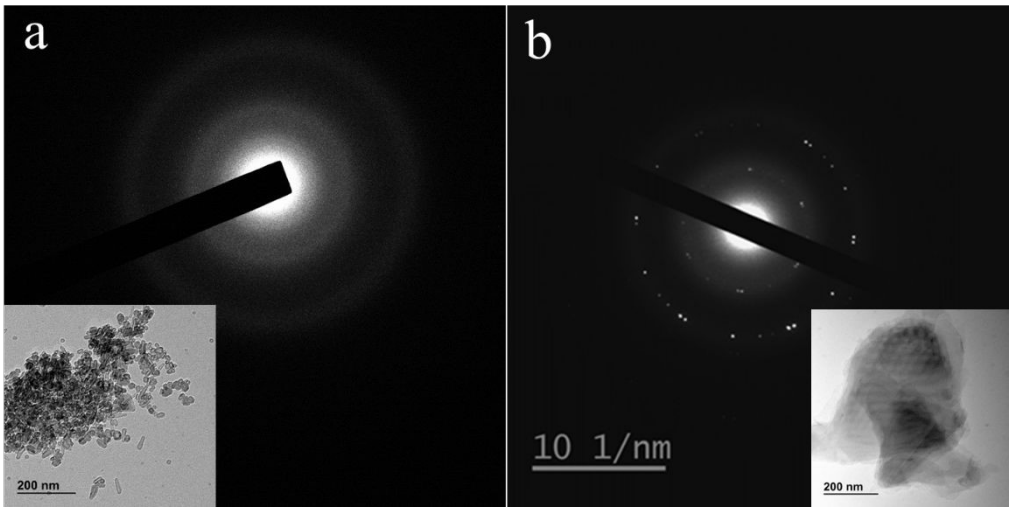

Figure 6: Electron diffraction patterns of carbon nanospheres (a); carbon honeycomb-like layers (b).

3.6.2 X-ray photoelectron spectroscopy (XPS)

The chemical composition of the samples was determined by XPS. The XPS elemental survey spectrum of prepared sample, provided in Figure S6, confirms that carbon is the principal component. The other product nanomaterials exhibit very similar spectra. The elemental compositions determined by XPS for all the samples are provided in Table 5. In addition to carbon, signals from silicon and oxygen are also present, presumably originating from the substrate.

View Article Online
DOI: 10.1039/D6NA00126B

Table 5. Elemental composition as determined by XPS.

Sample	Atomic quantity of elements (%)		
	C	O	Si
a	48.0	29.0	23.0
b	48.5	28.5	23.0
c	49.0	28.0	23.0
d	48.5	28.0	23.5

High-resolution C1s XPS spectra of the four samples are provided in Figure 7. Deconvolution indicates the presence of three primary components, centered at 284.6, 286.2 and 288.6 eV, respectively. The position of the most intense signal at 284.6 eV indicates that the majority (~70%) of carbon atoms in the samples are bonded to other carbon atoms and, furthermore, that most of the carbon-carbon bonds are double bonds.[33] The two other smaller peaks at 286.2 and 288.6 eV correspond to the carbon atoms bonded to oxygen, either through single or double bonds, respectively. It should be noted that signals at these positions also appear in the XPS spectra of the silicon wafer substrate and thus cannot be conclusively attributed to oxygen within the samples.

View Article Online
DOI: 10.1039/D6NA00126B

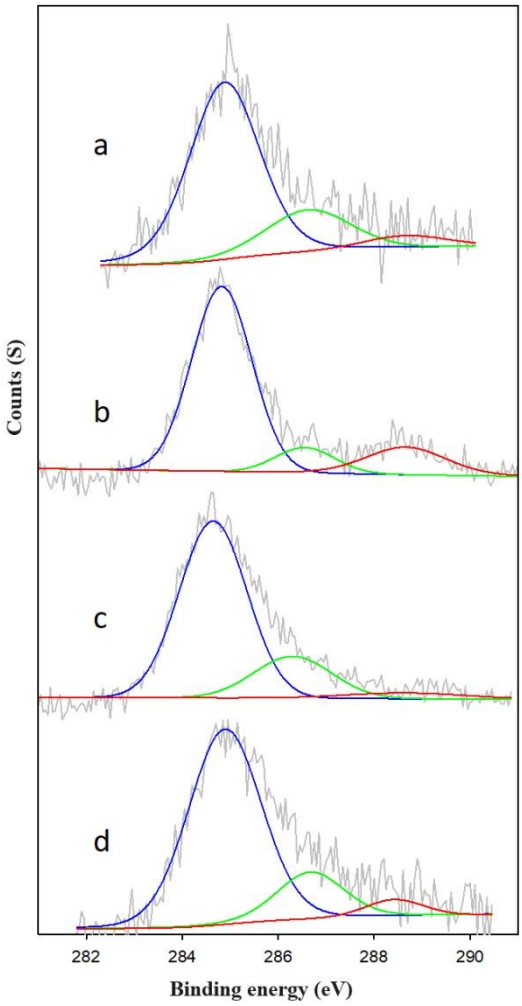

Figure 7. Deconvolution of the carbon 1s XPS signal obtained from samples **a**-**d**.

View Article Online
DOI: 10.1039/D6NA00126B

Table 6. Results of the XPS high resolution of carbon analysis.

Sample	XPS carbon binding energies /eV	Attribution	% Area
a	284.8 286.6 288.7	C=C C-O C=O	71 17 12
b	284.8 286.6 288.7	C=C C-O C=O	74 12 14
c	284.7 286.2 288.6	C=C C-O C=O	74 20 6
d	284.8 286.7 288.5	C=C C-O C=O	68 20 12

3.6.3 X-ray induced Auger electron spectroscopy (XAES)

XAES analysis has been reported as a method for determining the hybridization state of carbon [34]. More specifically, the degree of separation between the most positive maximum and the most negative minimum of first derivative of the carbon KLL Auger peaks, defined as the D parameter[34],

View Article Online
DOI: 10.1039/D6NA00126B

has been shown to vary linearly with the fraction of sp^2 hybridized carbon atoms. Auger C KLL spectra were recorded for the various carbon nanomaterials and are provided in the form of their first derivatives in Figure 8. To establish a calibration plot for sp^2 content as a function of the D parameter, graphite and polyethylene were selected as standards corresponding to 100% sp^2 and 100% sp^3 materials, respectively. The D value was experimentally evaluated as 19 eV for graphite (representing 100% sp^2 carbon) and 13.6 eV for polyethylene (representing 100% sp^3 carbon). The D parameters for the various carbon nanomaterials are provided in Table 7 along with the corresponding values for their sp^2 content. The results indicate that the materials have sp^2 contents ranging from 40 to 60%, with the carbon lamellar structure having the highest sp^2 hybridization content. It should be noted that care must be taken in the interpretation of these values since they will be influenced by contributions from carbon contaminants on the silicon wafer substrate. In fact, electron diffraction data indicate that sample **c** is composed of highly crystalline graphene sheets and the true sp^2 content is thus probably higher than 60%.

View Article Online
DOI: 10.1039/D6NA00126B

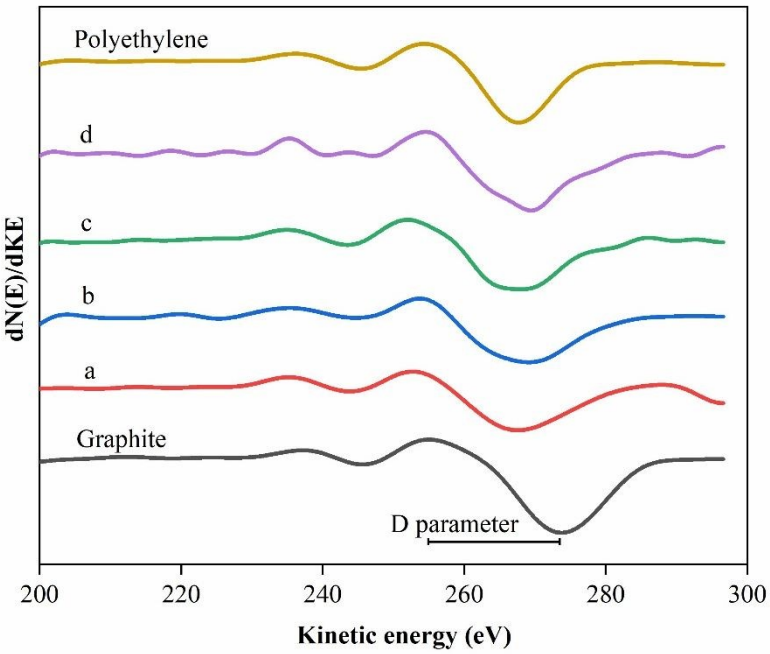

Figure 8: First-derivative C KLL Auger spectra recorded for different carbon nanostructures.

Table 7. D parameter and sp^2 value for all carbon nanostructures.

Sample	Auger D parameter / eV	sp^2 (%)
a	16	44
b	16	44
c	16.4	52
d	16	44
Graphite	19.0	100
Polyethylene	13.6	0

View Article Online
DOI: 10.1039/D6NA00126B

3.6.4 Raman spectroscopy

Raman spectroscopy was employed to evaluate the structural characteristics of the prepared carbon nanostructures. The Raman spectra of the prepared carbon nanomaterials are presented in Figure 9. All the spectra exhibit two bands, located at 1340–1360 cm^{-1} and 1550–1600 cm^{-1}, respectively. In addition, a broad signal located at 3000 cm^{-1} is observed in the spectrum of sample **c**, which, according to electron diffraction measurements, is composed of twisted graphene sheets.

The Raman signal observed at 1550–1600 cm^{-1} can be identified as the G-band, which arises from the in-plane vibration of sp^2-bonded carbon atoms and is a signature feature of graphitic materials. The presence of the G-band confirms the high sp^2 content of all the samples, consistent with the XPS and XAES results. The Raman signal observed around 1340–1360 cm^{-1} can be assigned to the D-band which is associated with a double-resonance (breathing mode) of carbon atoms in hexagonal ring structure[35]. Importantly, the D-band arises from defects within the lattice or at grain boundaries and is typically absent in highly ordered graphene and graphite structures[36]. Because of this, a sharp G-band and a low ratio of the intensities of the two bands, I(D)/I(G), are indicative of high structural regularity in carbon materials. The positions of the D- and G-bands, their relative intensities and full widths at half maximum height (FWHM) are provided in Table 8 for the various carbon nanomaterials.

Comparison of the Raman data for the various samples reveals that sample **c** differs from the others in the position of the G-band, the I(D)/I(G) intensity ratio and the widths of both the D- and G-bands. Ferrari and Robertson[37] have provided a detailed analysis of the evolution of the Raman

View Article Online
DOI: 10.1039/D6NA00126B

spectrum of carbon materials as a function of increasing disorder from graphite to fully amorphous carbon. They reported that in transitioning from nanocrystalline graphite to low sp^3 amorphous carbon, the position of the G-band evolves from ~1600 cm^{-1} to ~1510 cm^{-1}. The G-band position of sample **c** therefore agrees very well with the identification of this sample as being composed of highly crystalline, few-layer graphene. It should also be noted that, although the Raman spectrum of stacked graphene does vary somewhat with the number of layers, above five layers it is difficult to distinguish between the spectrum of few-layer graphene and that of graphite[35]. The G-band positions of the remaining samples (**a**, **b** and **d**) are consistent with the characterization of these nanomaterials as being composed of amorphous, high sp^2-content carbon.

As noted above, the intensity ratio I(D)/I(G) can be employed to assess the structural order of graphene[38]. In the case of single layer graphene, Jorio *et al.*[38] provided a quantitative correlation between the I(D)/I(G) ratio and the average distance between defects. According to their data, a I(D)/I(G) ratio of less than one corresponds to an average distance between defects on the order of 10 nm or greater. The intensity ratios reported in Table 8 therefore imply that graphene-like domains within the materials extend over many aromatic rings. However, since the samples investigated here are not composed of single-layer graphene, comparison with the data of Jorio *et al.*[38] must be accompanied by considerable reserve.

The linewidths of both the G- and D- bands are indications of disorder. The G-band in defect-free materials typically has a FWHM of 10-15 cm^{-1}, but this value increases with induced strain[36]. The D-band linewidth is highly sensitive to disorder and can vary from 7 cm^{-1} for isolated SWNTs to hundreds of wavenumbers for very defective carbon materials[39]. While the FWHM values

View Article Online
DOI: 10.1039/D6NA00126B

reported in Table 8 therefore indicate the presence of disorder within the samples, it is impossible to provide a quantitative analysis. Interestingly, sample **c** exhibits the narrowest bands, consistent with the crystalline nature of this sample.

Finally, sample **c** exhibits a broad 2D-peak in the Raman spectrum centered near 3000 cm^{-1}. The 2D-band is a second-order Raman signature observed for all sp^2 carbons[39] that are known to be highly sensitive to the number of graphene layers. In monolayer graphene, this peak typically appears sharp, symmetric, and of high intensity. However, in the case of a few-layer graphene (up to five layers), the 2D band becomes progressively broader and asymmetrical. The observed shape and moderate intensity of the 2D peak in sample **c** suggest the presence of multilayer graphene sheets, rather than a monolayer structure. This conclusion agrees well with the TEM images and electron diffraction pattern observed for this sample.

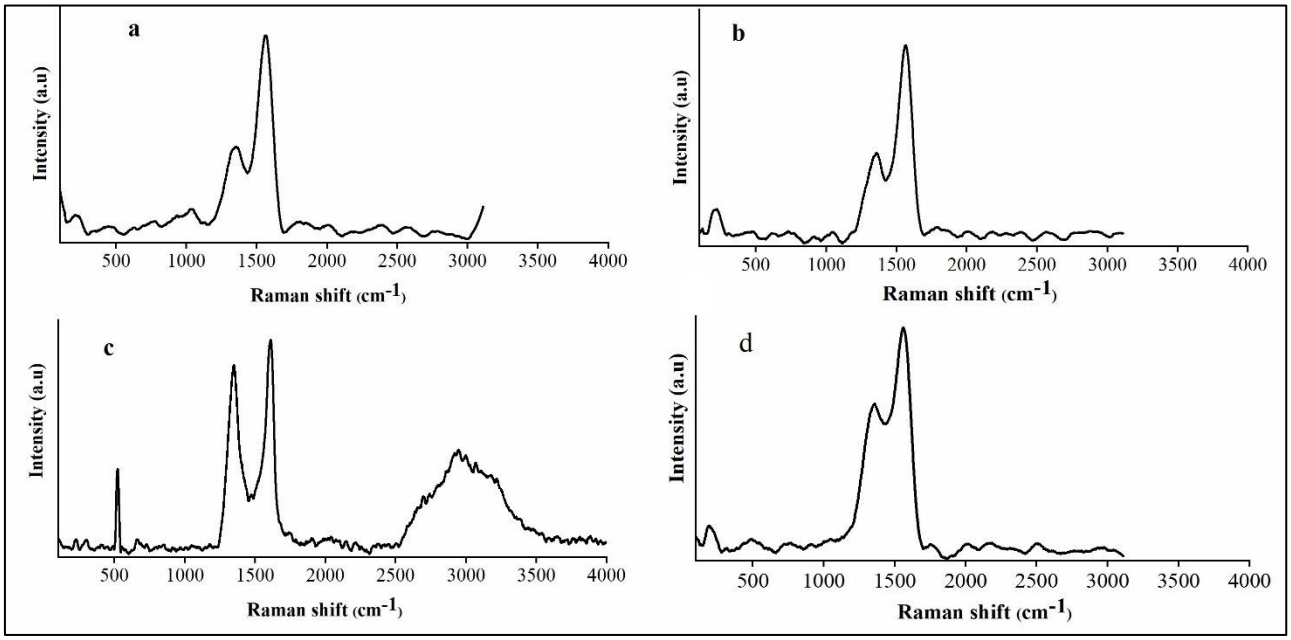

View Article Online
DOI: 10.1039/D6NA00126B

Figure 9: Raman spectra of prepared carbon nanomaterials: carbon nanospheres (a), carbon nanorods (b), carbon nanosheets (c), mixture of nanospheres and nanorods. Figure 9c was reproduced from reference 23 with permission from the American Chemical Society.

Table 8. Position, FWHM values, and the relative intensity, I(D)/I(G), of the Raman D and G bands for the prepared carbon nanostructures.

Sample	D band/cm^{-1}	FWHM/cm^{-1} D-peak	G band/cm^{-1}	FWHM/cm^{-1} G-peak	I(D)/I(G)
a	1347	134	1558	102	0.4
b	1347	134	1559	95	0.4
c	1348	89	1597	66	0.9
d	1362	149	1556	106	0.6

3.7 Summary of the results from various characterization methods

XPS, XAES and Raman spectroscopy all provide information about the nature of carbon-carbon bonding and hybridization. For the sake of comparison, the primary observations and conclusions from the three methods are summarized in Table 9. Overall, there is very good agreement between the various techniques; all indicate that the nanostructures are primarily composed of sp^2 hybridized carbon in the form of aromatic rings. XPS and XAES allow for the quantitative evaluation of sp^2 content and yield values on the order of 70% and 45%, respectively. Although at first sight the agreement between these two values may appear to be poor, the contribution of

View Article Online
DOI: 10.1039/D6NA00126B

carbon contaminants must also be considered. In fact, the TEM and electron diffraction results obtained for sample **c** indicate the presence of highly crystalline graphene layers and therefore suggest that the sp^2 content evaluated by XPS and XAES is underestimated.

Table 9. Summary of characterization results.

Characterization method	Observation	Interpretation
XPS	Primary C1s signal (74%) at 284.7 eV	Samples composed primarily (> 70%) of sp^2 C=C bonds
XAES	D value of 16 eV	Samples composed of 45-50% sp^2-hybridized carbon
Raman	Presence of D- and G-bands	Samples composed of carbon in an aromatic graphite/graphene structure
	Presence of broad asymmetric 2D-band for sample **c**	Sample composed of a small number of graphene layers
IR	Band at 1650 cm^{-1}	Aromatic C=C stretching

3.8 Reproducibility of the synthesis

The syntheses were repeated in triplicate at each template composition (**a**, **b**, **c** and **d**) and consistently yielded the same nanomaterial shape (hollow spheres, hollow rods, lamellae and a mixture of spheres and rods). In addition, the synthesis was repeated at each micellar composition with copper (II) fluoride rather than copper triflate as the source of the Cu^{2+} catalyst. TEM images

View Article Online
DOI: 10.1039/D6NA00126B

of the resulting materials are presented in Figure S7 and clearly illustrate the reproducibility of the method and its generality with respect to the copper source.

4. CONCLUSION

We report an entirely new, room temperature synthetic route to carbon nanomaterials. This approach relies on the use of a self-assembled surfactant template and yields hollow spheres, hollow cylinders or lamellae, depending on the exact composition of the template mixture. The observed correlation between the shape of the surfactant structures and the morphology of the synthesized carbon nanomaterials confirms the critical role of the templates in directing nanostructure formation. This observation, combined with the size and hollow nature of the spheres and rods provides convincing evidence that the initial step of the synthesis involves the polymerization of butadiyne at the water-organic interface of the template. We propose that the polymerization produces unstable polyynes that subsequently decompose to form solid, carbon nanomaterials. Furthermore, XPS, XAES and Raman spectroscopy indicate that the materials are primarily composed of sp^2 hybridized carbon arranged into aromatic rings. In the specific case of the use of a lamellar template, TEM and electron diffraction results reveal that highly crystalline, stacked graphene sheets are obtained.

This finding highlights the potential of soft-template methods as a versatile and controllable approach for designing carbon nanomaterials with specific and predictable shapes, which is essential for tailoring their properties for targeted applications in areas such as catalysis, energy storage, and nanomedicine.

View Article Online
DOI: 10.1039/D6NA00126B

ASSOCIATED CONTENT

Supporting Information. DLS, TEM, EDS, and XPS. This material is available free of charge via the Internet at http://pubs.acs.org.

AUTHOR INFORMATION

Corresponding Author

Jean-François Morin – *Département de chimie and Centre de Recherche sur les Matériaux Avancés (CERMA), Université Laval, Québec, Canada G1V 0A6;* orcid.org/0000-0002-9259-9051; Email: jean-francois.morin@chm.ulaval.ca

Anna M. Ritcey – *Département de chimie and Centre de Recherche sur les Matériaux Avancés (CERMA), Université Laval, Québec, Canada G1V 0A6;* orcid.org/ 0000-0002-9273-8525; Email: anna.ritcey@chm.ulaval.ca

Author Contributions

A.M.R. and J.-F.M. conceived and designed the project; S.J. conducted synthesis and completed the identification and con-tributed to the manuscript; All authors discussed the results and commented on the manuscript.

Funding Sources

View Article Online
DOI: 10.1039/D6NA00126B

This work was supported by the Fonds de recherche du Québec through its Team research project program under grant #254690.

Conflicts of interest

There are no conflicts to declare.

Notes

The authors declare no competing financial interest.

ACKNOWLEDGMENT

The authors would like to thank Dr. Pascale Chevallier for her help with XPS analysis, and M. Alexandre Bastien for his help with electron diffraction experiments. This work was supported by the Fonds de recherche du Québec through its Team research project program under grant #254690.

REFERENCES

1 N. Choudhary, S. Hwang and W. Choi, in *Handbook of Nanomaterials Properties*, Springer Berlin Heidelberg, 2014, pp. 709–769.

2 Y. Wang and A. Hu, *J. Mater. Chem. C*, 2014, **2**, 6921–6939.

3 A. Sharma and J. Das, *J. Nanobiotechnology*, 2019, **17**, 92.

4 H. Peng and J. Travas-Sejdic, *Chem. Mater.*, 2009, **21**, 5563–5565.

View Article Online
DOI: 10.1039/D6NA00126B

5 S. Liu, J. Tian, L. Wang, Y. Zhang, X. Qin, Y. Luo, A. M. Asiri, A. O. Al-Youbi and X. Sun, *Adv. Mater.*, 2012, **24**, 2037–2041.

6 S. Sahu, B. Behera, T. K. Maiti and S. Mohapatra, *Chem. Commun.*, 2012, **48**, 8835–8837.

7 P. C. Hsu, Z. Y. Shih, C. H. Lee and H. T. Chang, *Green Chem.*, 2012, **14**, 917–920.

8 G. G. A. Ozin and A. Arsenault, *Nanochemistry: a chemical approach to nanomaterials*, Royal Society of Chemistry, 2015.

9 Z.-G. G. Z. Gu, D.-J. J. D. Li, C. Zheng, Y. Kang, C. Wöll and J. Zhang, *Angew. Chemie*, 2017, **56**, 6957–6962.

10 S. F. Soares, T. Fernandes, A. L. Daniel-Da-Silva and T. Trindade, *Proc. R. Soc. A*, 2019, **475**, 20180677.

11 J. Wang, G. Liu, K. Leung, R. Loffroy, P.-X. Lu and Y. J. Wáng, *Curr. Pharm. Des.*, 2015, **21**, 5401–5416.

12 M. M. M. Wan, Z. Z. Wei, Z. Z. Zhang, L. L. Zhang, K. Huang and Y. Yang, *Synth. Met.*, 2003, **135**, 175–176.

13 Z.-G. G. Wang and B. Ding, *Adv. Mater.*, 2013, **25**, 3905–3914.

14 X. Zhang and S. K. Manohar, *Chem. Commun.*, 2004, 2360–2361.

15 L. Huang, Z. Wang, H. Wang, X. Cheng, A. Mitra and Y. Yan, *J. Mater. Chem.*, 2002, **12**, 388–391.

View Article Online
DOI: 10.1039/D6NA00126B

16 J. Jang and H. Yoon, *Chem. Commun.*, 2003, **3**, 720–721.

17 X. Zhang, J.-S. S. Lee, G. S. Lee, D.-K. K. Cha, M. J. Kim, D. J. Yang and S. K. Manohar, *Macromolecules*, 2006, **39**, 470–472.

18 J. D. Hopwood and S. Mann, *Chem. Mater.*, 1997, **9**, 1819–1828.

19 H. Shi, L. Qi, J. Ma and H. Cheng, *J. Am. Chem. Soc.*, 2003, **125**, 3450–3451.

20 S. Kumar, V. Singh, S. Aggarwal and U. Kumar Mandal, *Colloid Polym. Sci.*, 2009, **287**, 1107–1110.

21 C. H. Lin, J. J. H. Chang, Y. Y. Q. Yeh, S. S. H. Wu, Y. Y. H. Liu, C. M.- Nanoscale, undefined 2015 and C. Y. Mou, *Nanoscale*, 2015, **7**, 9614–9626.

22 A. Rajapantulu and R. Bandyopadhyaya, *Langmuir*, 2021, **37**, 6623–6631.

23 S. Jahani, J. F. Morin and A. M. Ritcey, *ACS Appl. Nano Mater.*, 2025, **8**, 17952–17958.

24 E. T. Chernick and R. R. Tykwinski, *J. Phys. Org. Chem.*, 2013, **26**, 742–749.

25 S. Schrettl, C. Stefaniu, C. Schwieger, G. Pasche, E. Oveisi, Y. Fontana, A. F. I. Morral, J. Reguera, R. Petraglia, C. Corminboeuf, G. Brezesinski and H. Frauenrath, *Nat. Chem.*, 2014, **6**, 468–476.

26 N. S. Goroff, *J. Am. Chem. Soc.*, 2006, **128**, 8987–8987.

27 G. E. Jones, D. A. Kendrick and A. B. Holmes, *Org. Synth.*, 1987, **65**, 52.

View Article Online
DOI: 10.1039/D6NA00126B

28 I. Lisiecki, P. André, A. Filankembo, C. Petit, J. Tanori, T. Gulik-Krzywicki, B. W. Ninham and M. P. Pileni, *J. Phys. Chem. B*, 1999, **103**, 9168–9175.

29 I. Lisiecki, P. André, A. Filankembo, C. Petit, J. Tanori, T. Gulik-Krzywicki, B. W. Ninham and M. P. Pileni, *J. Phys. Chem. B*, 1999, **103**, 9176–9189.

30 E. Álvarez, L. García-Río, J. C. Mejuto, J. M. Navaza and J. Pérez-Juste, *J. Chem. Eng. Data*, 1999, **44**, 850–853.

31 R. Nagarajan, *Langmuir*, 2002, **18**, 31–38.

32 D. Lombardo, M. M. A. Kiselev, S. Magazù, P. Calandra, … S. M.-A. in C. and U. 2015, *Adv. Condens. Matter Phys.*, 2015, **2015**, 151683.

33 B. Lesiak, L. Kövér, J. Tóth, J. Zemek, P. Jiricek, A. Kromka and N. Rangam, *Appl. Surf. Sci.*, 2018, **452**, 223–231.

34 S. Y. Lee, J. Lyu, S. Kang, S. J. Lu and C. W. Bielawski, *J. Phys. Chem. C*, 2018, **122**, 11855–11861.

35 A. C. Ferrari, *Solid State Commun.*, 2007, **143**, 47–57.

36 V. Thapliyal, M. E. Alabdulkarim, D. R. Whelan, B. Mainali and J. L. Maxwell, *Diam. Relat. Mater.*, 2022, **127**, 109180.

37 A. Ferrari and J. Robertson, *Phys. Rev. B - Condens. Matter Mater. Phys.*, 2000, **61**, 14095–14107.

View Article Online
DOI: 10.1039/D6NA00126B

38 A. Jorio, E. H. M. Ferreira, M. V. O. Moutinho, F. Stavale, C. A. Achete and R. B. Capaz, *Phys. Status Solidi Basic Res.*, 2010, **247**, 2980–2982.

39 A. Jorio, *ISRN Nanotechnol.*, 2012, **2012**, 1–16.

View Article Online
DOI: 10.1039/D6NA00126B

Data Availability

The data that support the findings of this study are available from the corresponding author, Prof. Jean-François Morin (jean-francois.morinhm.ulaval.ca), upon reasonable request.